Published online 1 April 2016

Nucleic Acids Research, 2016, Vol. 44, No. 8 ***3763–3771***
doi: 10.1093/nar/gkw196

Quantifying the ion atmosphere of unfolded, single-stranded nucleic acids using equilibrium dialysis and single-molecule methods

David R. Jacobson[1] and Omar A. Saleh[2]

[1]Department of Physics, University of California, Santa Barbara, CA 93106, USA and [2]Materials Department and BMSE Program, University of California, Santa Barbara, CA, USA

Received January 04, 2016; Revised March 06, 2016; Accepted March 14, 2016

ABSTRACT

To form secondary structure, nucleic acids (NAs) must overcome electrostatic strand–strand repulsion, which is moderated by the surrounding atmosphere of screening ions. The free energy of NA folding therefore depends on the interactions of this ion atmosphere with both the folded and unfolded states. We quantify such interactions using the preferential ion interaction coefficient or ion excess: the number of ions present near the NA in excess of the bulk concentration. The ion excess of the folded, double-helical state has been extensively studied; however, much less is known about the salt-dependent ion excess of the unfolded, single-stranded state. We measure this quantity using three complementary approaches: a direct approach of Donnan equilibrium dialysis read out by atomic emission spectroscopy and two indirect approaches involving either single-molecule force spectroscopy or existing thermal denaturation data. The results of these three approaches, each involving an independent experimental technique, are in good agreement. Even though the single-stranded NAs are flexible polymers that are expected to adopt random-coil configurations, we find that their ion atmosphere is quantitatively described by rod-like models that neglect large-scale conformational freedom, an effect that we explain in terms of the competition between the relevant structural and electrostatic length scales.

INTRODUCTION

The formation of secondary structure through Watson–Crick base pairing is essential to the structure and function of RNA and DNA in both biology (e.g. RNA ribozymes (1) and riboswitches (2)) and biotechnology (e.g. DNA origami (3)). Both species of nucleic acid (NA) are strongly negatively charged, and so in forming double-stranded helices they must overcome significant electrostatic (ES) repulsion. This is accomplished through screening of the ES potential by counterions specifically bound to the NA structure (as in the case of chelated divalent ions) or loosely associated in an ion atmosphere (4). To fully account for the ES free energy of secondary structure formation, we require a quantitative description of the association of ions with both the folded, helical state and the unfolded, single-stranded state.

A number of studies have probed the stoichiometry of ion association with double-stranded DNA (5–10). For salt species with high mean ion activity coefficients (e.g. NaCl), these results can be modelled by solutions to the non-linear Poisson–Boltzmann (NLPB) equation (10). Much less is known about the interaction of ions with unfolded, single-stranded NAs (ssNAs): some early papers (11–13) have reported changes in counterion activity as a DNA helix is thermally or chemically denatured and, more recently, anomalous small-angle X-ray scattering (ASAXS) results have quantified the ion atmosphere of a single-stranded DNA oligonucleotide at one particular concentration of RbCl salt (14).

Here, we rigorously measure the stoichiometry of ion association with single-stranded DNA and RNA using three independent, complementary techniques: the first a direct equilibrium dialysis experiment, the other two indirect thermodynamic cycle analyses using the known double-stranded results in combination with either single-molecule magnetic tweezer experiments or existing thermal denaturation data. The salt-dependent results that we obtain by all three methods are in good agreement. We then identify the relevant physical parameters underlying the observed behaviour by comparing the results to models of the ion atmosphere incorporating varying amounts of structural and conformational detail.

Quantifying the ion atmosphere

The various NA conformational states are related through the thermodynamic cycle depicted in Figure 1, where the

*To whom correspondence should be addressed. Tel: +1 805 893 8814; Fax: +1 805 893 8486; Email: saleh@engineering.ucsb.edu

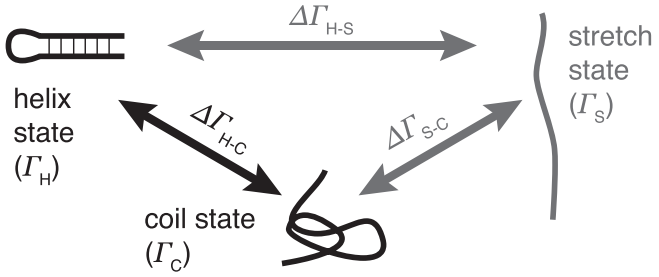

Figure 1. Thermodynamic cycle diagram for mechanical unfolding of an NA hairpin. The helix state refers to the intact hairpin, the stretch state to the hairpin after being mechanically unfolded by an applied force and the coil state to the unfolded hairpin in the absence of force. Each state is characterized by a salt-dependent preferential cation interaction coefficient (ion excess), Γ_i, and each transition is associated with a change in ion excess, $\Delta\Gamma_{i-j}$.

helix state refers to the double-stranded NAs (dsNAs) and the coil state refers to the flexible ssNAs. The stoichiometry of cation interactions with each state is quantified using the preferential cation interaction coefficient Γ, defined in terms of either molal or molar units: (4,15)

$$\Gamma^{\text{molal}} = \lim_{m_0 \to 0} \left(\frac{\partial m_+}{\partial m_0} \right)_{\mu_+}, \tag{1}$$

$$\Gamma^{\text{molar}} = \lim_{c_0 \to 0} \left(\frac{\partial c_+}{\partial c_0} \right)_{\mu_+}, \tag{2}$$

where the subscript μ_+ denotes constant ion chemical potential and m_+ (c_+) and m_0 (c_0) denote the molal (molar) concentrations of the cation species and the NA, respectively. In the dilute NA limit, Γ can be interpreted as the *ion excess*: the number of ions present in the vicinity of the NA beyond the number that would be expected due to the bulk concentration alone. There is a subtlety in distinguishing between the molal and molar concentration units of Equations (1) and (2) (10,16). Concentrations measured in molal units (i.e. constant solvent volume) are most easily interpreted and give simple high- and low-salt limiting behaviours that derive from the electrostatics of the system, as discussed below. However, the dialysis experiments we present in this paper naturally report molar concentrations (i.e. constant total solution volume). In these units, Γ^{molar} includes both a positive contribution due to the excess ions surrounding the NA and a negative contribution due to the ions excluded from the NA's occupied volume. Since this molar excluded volume (EV) effect obscures, at high-salt concentration, the ES effects we aim to study, we will report raw, molar data, but will also use EV-corrected, molal results when comparing with electrostatics-derived theoretical models. In both cases, these ion excesses will be normalized on a per-nucleotide basis, denoted $\bar{\Gamma}$.

The negative charge of an NA is neutralized by a combination of two effects: a positive cation excess and a negative anion excess (i.e. cation association and anion exclusion). To understand the dependence of the ion excess on the bulk salt concentration, c, it is useful to identify high- and low-salt limiting behaviours. When working in molal units, these limits can be straightforwardly evaluated in terms of solution electrostatics. The low-salt limit is derived based on Manning counterion condensation theory and the Poisson–Boltzmann equation (17,18). In terms of the Manning parameter $\xi = l_B/b$, where l_B is the Bjerrum length and b is the charge spacing along the NA helical axis, this theory predicts that

$$\lim_{c \to 0} \bar{\Gamma}^{\text{molal}} = \begin{cases} 1/2 + \xi/4 & \xi < 1 \\ 1 - 1/(4\xi) & \xi > 1 \end{cases}. \tag{3}$$

Based on the charge densities of the NAs under consideration (19), Equation (3) predicts $\bar{\Gamma}^{\text{molal}} \to 0.94$ for dsDNA, 0.75 for ssDNA, 0.96 for dsRNA and 0.79 for ssRNA, assuming a thin-cylinder geometry. Since the EV effect is unimportant at low-salt concentration, these limiting results are also expected to hold when working in molar units. In the high-salt limit, strong screening reduces the ES potential to the Debye–Hückel (linear Poisson–Boltzmann) limit (20) and $\bar{\Gamma}^{\text{molal}} \to 0.5$ (21). In other words, the potential is sufficiently weak that it acts equally and oppositely between all charge pairs and the macromolecule's charge is equally offset by association of cations and exclusion of anions. When working in molar units—that is to say, in our experiments—this limit is washed out by volume-excluded ions, which increase linearly in number with increasing salt, leading to a linear decrease in Γ^{molar} (see Supplementary Figure S8) (10,22). At the intermediate salt concentrations of biological interest, Γ interpolates between these two limits. As Olmsted *et al.* have shown, however, this interpolation need not be monotonic, such as in the case of short oligonucleotides (23).

MATERIALS AND METHODS

Dialysis/atomic emission spectroscopy (D-AES)

We measured the ion excess of 50-mer homopolymeric oligonucleotides (Integrated DNA Technologies) of thymidine (DNA) and uridine (RNA), which do not form secondary structure or exhibit appreciable base stacking interactions (24,25). NA solutions (100 µl, 0.07–0.7 mM) were dialyzed against a 200 ml bulk reservoir of buffer containing 1 mM MOPS, adjusted to pH 7 with NaOH, and the desired concentration of NaCl. A dialysis membrane with a 6–8 kDa molecular weight cutoff was used (D-Tube Dialyzer Mini, EMD Millipore). After 5 h of stirring, samples were taken of both the NA and bulk solutions and diluted with pure water to concentrations in the range of sensitivity of the AES spectrometer.

The Na^+ ion excess per nucleotide, $\bar{\Gamma}_C$, is determined from the molar concentrations of sodium in the NA solution, $c_{\text{Na}}^{\text{sample}}$, and in the bulk, $c_{\text{Na}}^{\text{bulk}}$, and from the concentration of nucleotides, $c_{\text{P}}^{\text{sample}}$: (7)

$$\bar{\Gamma}_C^{\text{molar}} = \frac{c_{\text{Na}}^{\text{sample}} - c_{\text{Na}}^{\text{bulk}}}{c_{\text{P}}^{\text{sample}}}. \tag{4}$$

The various concentrations were measured using inductively coupled plasma atomic emission spectroscopy (AES) (iCAP 6300, Thermo Scientific) calibrated using standard solutions of sodium and phosphorus (Fluka). The details

of the calibration are given in the Supplementary Data. To keep the measurement uncertainty in the Γ_C results reasonably small, it is necessary to increase the sample NA concentration as the bulk salt concentration is increased. Comparison of data obtained at different NA concentrations shows no concentration dependence; nonetheless, we were careful always to stay well below the solution overlap concentration: approximately 3.5 mM at low $c_{\mathrm{Na}}^{\mathrm{bulk}}$, based on salt-dependent persistence lengths from the FRET experiments of Chen *et al.* (26). Because we noticed a correlation between samples from separate dialysis runs read out in the same AES batch, we use the number of such batches, and not the total number of samples, in computing the reported standard errors of the mean. Each reported D-AES datum represents the results of at least three dialysis experiments, each read out by AES at least twice.

NLPB calculations

We used NLPB calculations to estimate the ion excess of the helix state, Γ_H, using model A-form or B-form helices for RNA or DNA, respectively. These same helices with one strand removed were used as naive models of the ssNAs. Calculations were carried out using the Adaptive Poisson–Boltzmann Solver (27) over a range of NaCl concentrations. Structural models were obtained from the Nucleic Acid Builder (28) and charges were assigned using the PDB2PQR package (29,30). The detailed parameters used are given in the Supplementary Data. Although we use atomically resolved structural models here, Shkel and Record have demonstrated that comparable results can be obtained for NA thermodynamic properties using cylindrical models (31). Ion excess values were obtained in both molal (7) and molar (10,16) units by appropriate integration of the resulting ion densities.

Single-molecule magnetic tweezers studies

The change in ion excess, $\Delta\Gamma_{H-S}$, as an RNA hairpin is mechanically unfolded was determined by measuring the salt-dependent unfolding force using magnetic tweezers (32) and then applying a thermodynamic argument (33–37). The molecular construct (Figure 2A, Supplementary Figure S2) consisted of a 25 base pair RNA hairpin closed by a hexaethylene glycol (HEG) loop (Integrated DNA Technologies), separated from the glass surface of the flow cell by an 828 base pair double-stranded DNA spacer and from the magnetic bead by dT_{20} single-stranded DNA. The uncharged HEG loop was used instead of an RNA loop to isolate the ES effects of the helix from those of the loop. Experiments were carried out in 10 mM MOPS buffer, adjusted to pH 7.5, and in various concentrations of NaCl determined by weight. Control experiments were performed to show that the $\Delta\Gamma$ results are insensitive to the nature of the hairpin-closing loop and to the cationic versus anionic nature of the buffer (4) (except at very low salt, $c < 25$ mM). The results of these control experiments, and a more detailed description of the molecular construct, are given in the Supplementary Data.

The thermodynamic argument used to extract $\Delta\Gamma_{H-S}$ is summarized below and fully explained elsewhere (34). We begin with a thermodynamic identity connecting changes in the relevant free energy for magnetic tweezers experiments, the grand canonical (Landau) potential of mean extension, $d\Omega$, and changes in the experimental parameters X (molecular extension), f (applied force), Γ_i (excess of a particular species of ion) and μ_i (chemical potential of that ion in bulk solution):

$$d\Omega = -Xdf - \sum_{\text{species}} \Gamma_i d\mu_i. \tag{5}$$

In an experiment, f and μ are directly controlled and X is measured; therefore, Equation (5) can be used to derive several relations to extract $\Delta\Gamma$, the change in ion excess between conformational states, from the experimental data (34). In this paper, we report results using one of these methods, a generalized Clausius–Clapeyron relation, although we show in Supplementary Figure S6 that the results of the other methods are in agreement. This Clausius–Clapeyron relation is given by

$$\Delta\Gamma = \frac{\Delta X}{2k_B T\alpha}\left(\frac{\partial f_c}{\partial \ln c}\right), \tag{6}$$

where ΔX is the change in extension between the folded and unfolded states, f_c is the equilibrium unfolding force of the hairpin, c is the bulk molar salt concentration and α is the concentration-dependent activity correction factor tabulated in the supporting information of Dittmore *et al.* (33).

The salt-dependent values of f_c are extracted from two-state folding/unfolding trajectories as shown in Figure 2B. For each trace, collected at a particular c and constant f, a histogram is made and the equilibrium constant calculated as a ratio of occupancy times: $K = T_{\mathrm{folded}}/T_{\mathrm{unfolded}}$. For each salt concentration, $\ln K$ is plotted versus f and fit with a two-state Boltzmann model to obtain f_c. The derivative $(\partial f_c/\partial \ln c)$ in Equation (6) is evaluated separately for the f_c data of each trial, yielding $\Delta\Gamma_{H-S}$.

RESULTS

Coil ion excess measured by D-AES

We measured the ion excess of the unfolded coil state, $\Gamma_C^{\mathrm{molar}}$, directly using dialysis and atomic emission spectroscopy (D-AES). This method relies on the phenomenon of Gibbs–Donnan equilibrium (38), in which the NA solution is placed in grand canonical equilibrium, across a membrane, with a salt reservoir. Attractive interactions with cations, repulsive interactions with anions and EV effects all lead to perturbations in the molar ion concentrations in the sample compartment compared with the reservoir. These perturbations, which we measure by AES, yield $\Gamma_C^{\mathrm{molar}}$ through Equation (4). In these experiments we used 50 nucleotide NA homopolymers that do not exhibit appreciable secondary structure formation or base stacking (24,25). D-AES results for $\bar{\Gamma}_C^{\mathrm{molar}}$ of both dT_{50} DNA and rU_{50} RNA are shown in Figure 3. There is known to be a length dependence to the NA ion excess (23,39); as such, the results we present can only be extrapolated to NAs of other lengths through appropriate correction.

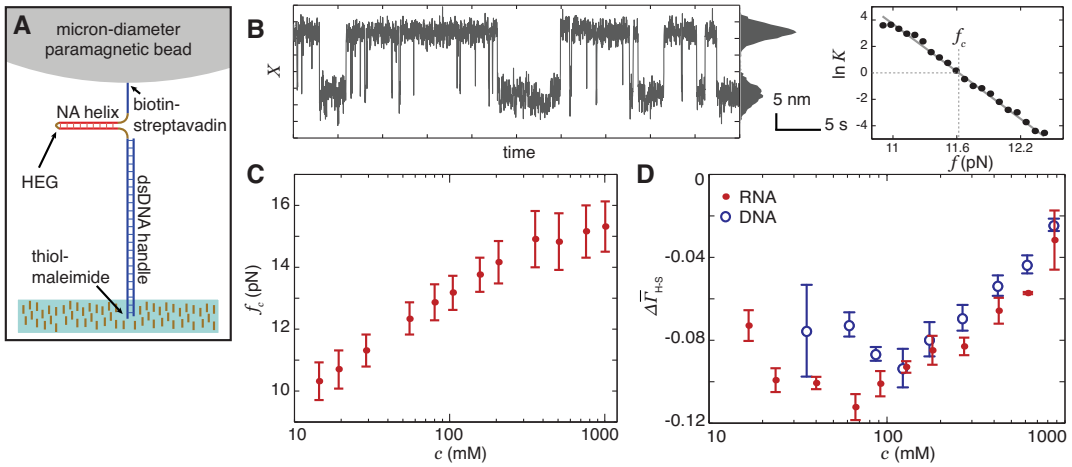

Figure 2. Single-molecule magnetic tweezers experiment to measure the the change in ion excess, $\Delta\bar{\Gamma}_{H-S}$, when an RNA hairpin is mechanically unfolded. (**A**) Diagram of the molecular construct. (**B**) Sample trace showing hopping between two conformational states, corresponding to two molecular extensions, X, and extraction of the corresponding equilibrium constant, K. The unfolding force, f_c, is then obtained from a plot of ln K versus applied force. (**C**) Plot of f_c as a function of bulk NaCl concentration for the RNA hairpin. (**D**) $\Delta\bar{\Gamma}_{H-S}$ for an RNA hairpin (points) and previously reported (33) values for a DNA hairpin (open circles) using the generalized Clausius–Clapeyron method. Error bars reflect standard errors of the mean.

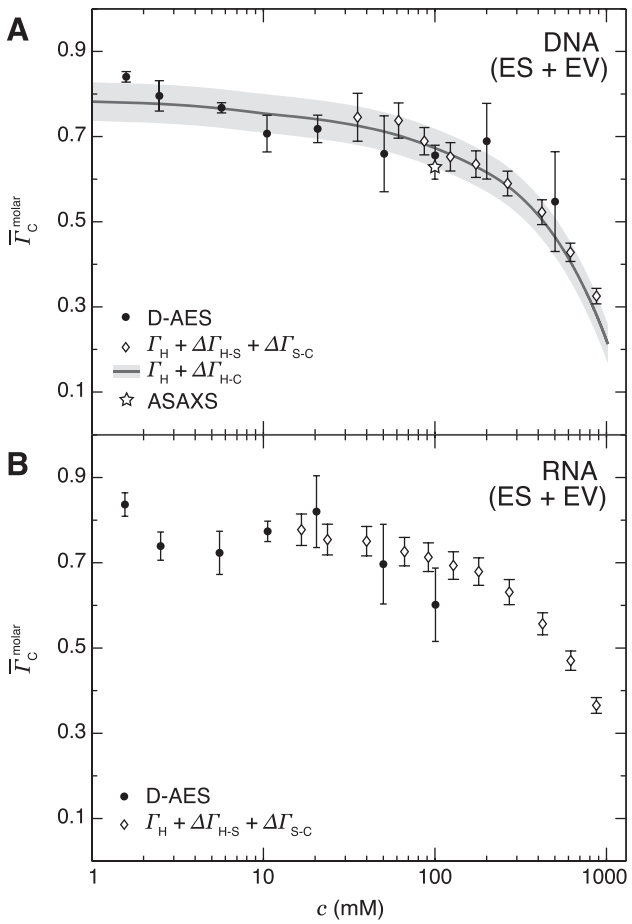

Figure 3. Values of $\bar{\Gamma}_C^{molar}$ (i.e. including both ES and EV effects) for (**A**) DNA and (**B**) RNA, determined directly by D-AES (solid points) and indirectly by thermodynamic cycle analysis using NLPB calculations and either single-molecule experiments (33,35,42) (open diamonds) or melting experiments (49) (line/shaded region). Also plotted is the DNA ASAXS result of Meisburger *et al.* (14) in RbCl (star).

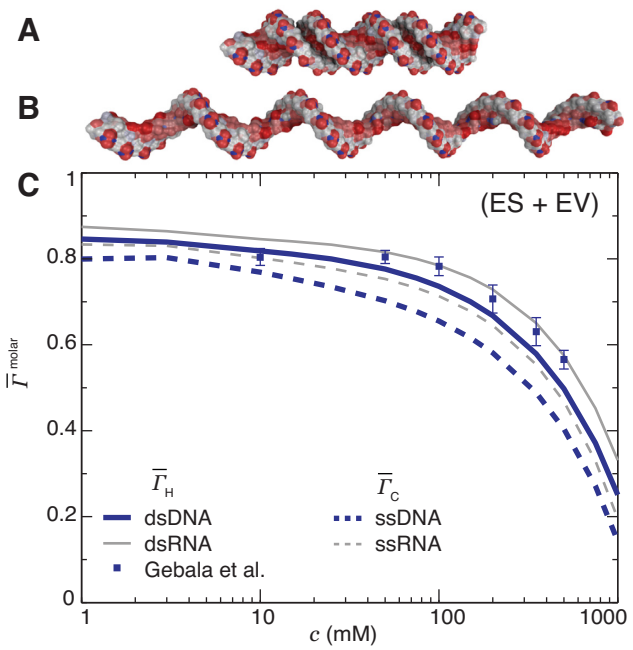

Figure 4. Structural model of dsDNA (**A**) and naive model of ssDNA (**B**) used in NLPB calculations, each having 50 nucleotides. Equivalent models for RNA were also used. (**C**) Ion excess of dsDNA (thick solid line) and dsRNA (thin solid line) in molar units, calculated by numerical evaluation of the NLPB equation as a function of bulk salt concentration. The use of NLPB to estimate $\bar{\Gamma}_H$ is validated by comparison with the experimental results of Gebala *et al.* (10) (squares). Similar NLPB results for models of the ssNA structure neglecting any conformational freedom are plotted for DNA (thick dashed line) and RNA (thin dashed line).

NLPB calculations

We obtain Γ_H, the ion excess of the folded, helical state, using numerical solutions to the NLPB equation on model A-form (RNA) and B-form (DNA, Figure 4A) double helices under various bulk salt concentrations. In using the

canonical double-helix geometries, we assume that the helices do not undergo significant conformational fluctuations over time or significant conformational changes between salt concentrations. Molecular dynamics simulations of dsDNA, which show no clear trend in various structural parameters with salt (40), support this assumption. In using the Poisson–Boltzmann equation, we assume that ion–ion effects are sufficiently weak that the ion density can be treated as a continuous mean field, which is well established in the case of monovalent ions (41). Agreement with experimental data further validates both assumptions. Figure 4C shows the results of our NLPB calculations, in molar units, for dsDNA and dsRNA as solid lines; co-plotted are the results of DNA buffer equilibration/AES studies that show reasonable agreement with the NLPB (10). That there is some disagreement, especially at high-salt, could arise from the non-ideal solution behaviour of NaCl; Gebala *et al.* have shown that NLPB calculations best reproduce experimental ion counting data for ion species with the highest mean ion activity coefficients (10). We use the average extent of this disagreement as an estimate of the NLPB error.

The dashed lines in Figure 4C show results of similar NLPB calculations for simple models of the ssNAs (i.e. the dsNA models with one strand removed, Figure 4B). We do not expect such models to truly capture the physics of the single-stranded system, as the flexible ssNAs exist in a conformational ensemble that is unsampled by these models. Shkel and Record have successfully used such modelling to explain some ssDNA properties (31). These naive models give a handle on certain local aspects of the problem: the effects of close co-localization of strands and of the charge spacing along the backbone. We see the first effect by comparing the dsNA and ssNA curves in Figure 4C: for a particular species and at a particular salt concentration, the ion excess of the ssNA is slightly lower than that of the dsNA (∼3–6% for DNA, 3–10% for RNA). This reduction is expected based on the reduced charge density of the single-stranded state, which puts the system closer to the Debye–Hückel limit. We see the second effect, that of the charge spacing along the backbone, by comparing the DNA and RNA curves. Because DNA has a greater charge spacing along the sugar-phosphate backbone than RNA (0.70 nm versus 0.59 nm) (19), it has a smaller local charge density and is thus also closer to this limit.

Single-molecule measurement of $\Delta\Gamma_{H-S}$

We use single-molecule magnetic tweezer experiments (32) to measure the mechanical force needed to unfold an RNA helix as a function of bulk salt concentration. The experimental geometry is sketched in Figure 2A and the method used to determine the equilibrium unfolding force, f_c, is illustrated in Figure 2B. We then apply a thermodynamic relation (34) to these $f_c(c)$ data to extract the change in ion excess associated with this unfolding, $\Delta\Gamma_{H-S}$.

Figure 2C plots the equilibrium unfolding force, f_c, for the RNA helix. We see that f_c increases linearly with $\ln c$ over low-to-moderate salt concentrations and flattens off as c approaches 1 M. Equation (6) is applied to these data to obtain $\Delta\bar{\Gamma}_{H-S}$, which is non-constant across most of the salt range studied (Figure 2D); similar results for DNA (33) are co-plotted. In both cases ions are released when the NA helix unfolds and, at sufficiently high salt, the number released decreases with increasing $\ln c$. This is consistent with a screening length argument. At high salt the Debye length becomes short enough that all charges on the macromolecule are electrostatically isolated; thus, the differences in charge arrangement between the helix and stretch states become unimportant and the difference in ion excess between the states, $\Delta\bar{\Gamma}_{H-S}$, goes to zero.

Completing the thermodynamic cycle

Starting from the Γ_H results of Figure 4C, an indirect measurement of Γ_C can be reached using either of two routes through the thermodynamic scheme of Figure 1: via single-molecule stretching experiments, in which

$$\Gamma_C = \Gamma_H + \Delta\Gamma_{H-S} + \Delta\Gamma_{S-C}, \tag{7}$$

or via oligonucleotide melting studies, in which

$$\Gamma_C = \Gamma_H + \Delta\Gamma_{H-C}. \tag{8}$$

Results can be obtained in either molar or molal units by using Γ_H values integrated in the appropriate way from the NLPB calculations.

Evaluation of the mechanical stretching method (Equation (7)) requires Γ_H and $\Delta\Gamma_{H-S}$, obtained as discussed above, and also $\Delta\Gamma_{S-C}$, the change in the ion excess as the stretched state is relaxed to a random coil without refolding. Prior studies have reported $\Delta\Gamma_{S-C}$ data for homopolymers of DNA (35) and RNA (42) that do not form secondary structure. These homopolymers were on the order of 1000 nucleotides in length, and may exhibit length-dependent effects when compared with the 50-mers we use in the present studies. An exact correction for such effects is not known to us, but would have only a minor effect: $\Delta\Gamma_{S-C}$ contributes only a few percent to the value of Γ_C. Also, whereas the previously reported $\Delta\Gamma_{S-C}$ values were obtained by fitting the data with a surface having a particular functional form, analyzing the data in a way that does not depend on the choice of model function leads us to conclude that, within uncertainty, $\Delta\Gamma_{S-C}$ is salt-independent. As such, we arrive at per-nucleotide $\Delta\bar{\Gamma}_{S-C}$ values of 0.027 ± 0.003 for RNA and 0.043 ± 0.005 for DNA. Using these results, we can then evaluate Equation (7) to obtain the first indirect evaluation of $\bar{\Gamma}_C$, which is plotted in molar units alongside the D-AES results in Figure 3.

Alternatively, we can complete the thermodynamic cycle using Equation (8), which relies on the NLPB results for Γ_H and also on $\Delta\Gamma_{H-C}$ data from oligonucleotide melting experiments (43–48). We are unaware of suitable data for RNA melting, so we confine our analysis by this method to DNA. Owczarzy *et al.* (49) have reported melting temperatures for DNA oligonucleotides as a function of length, base composition and salt concentration. We analysed all of the 25 base pair data in their dataset using

$$\Delta\Gamma_{H-C} = \frac{1}{2\alpha\beta}\frac{N-2}{N}\frac{dT_m}{d\ln c}, \tag{9}$$

which follows from Olmsted *et al.* (23), where T_m is the duplex melting temperature, N is the number of base pairs

and $\beta = RT_m^2/\Delta H^o$ is a compound constant measured by calorimetry of NA conformational transitions and having a value of $\beta = 55 \pm 10\%$ (50). Performing this analysis, the details of which are given in the Supplementary Data, gives $\Delta\Gamma_{H-C}$ over [NaCl] = 69-1025 mM. We extrapolate to lower salt concentrations by assuming constant $\Delta\Gamma_{H-C}$, an assumption that is supported by other melting experiments (50). Finally, we evaluate Equation (8) to obtain the second indirect measure of $\bar{\Gamma}_C$, which is also plotted, in molar units, in Figure 3A.

DISCUSSION

Despite being based on different experimental techniques, the various methods discussed above agree on a consistent trend in the salt dependence of the ion excess of random-coil, single-stranded DNA and RNA (Figure 3). The linear decrease in molar ion excess at high salt (see plot with linear axes, Supplementary Figure S8) is due to EV effects; ES effects, which are of greatest interest to understanding NA–ion interactions, manifest as perturbations to this behaviour. We can isolate the ES effects by correcting the data into molal units. This is done, for the thermodynamic cycle measurements, by using the molal values of Γ_H from the NLPB and, for the D-AES measurements, by adding an EV correction. This correction is obtained by multiplying the EV of the NA—estimated from the structural model of Figure 4B incorporating a Stern layer—by the bulk salt concentration. Such EV-corrected, molal data are plotted in Figure 5, where we now see that the data lie, roughly, between the expected low-salt Manning ($\bar{\Gamma} \to 0.75$–0.79, assuming thin-cylinder geometry) and high-salt Debye–Hückel ($\bar{\Gamma} \to 0.5$) limits. Below, we explore electrostatics models to quantitatively reproduce the $\Gamma_C^{\text{molal}}(c)$ curves between these limits.

Uniform mean-field model

Because the ssNAs are so flexible and exist in an ensemble of random-coil conformations, we hypothesized that the chain would act as a uniform charge distribution, with the charge density given by the average over all configurations. In a simple model of this picture, we treat the system as consisting of two compartments in Gibbs–Donnan equilibrium with each other: one a bulk reservoir and the other a region of uniform charge density, ρ. This charged region represents the NA coil, ignoring any effects that may arise from the shape of the NA or the discreteness of its charge. Following the derivation given in the Supplementary Data, we solve for the per-nucleotide cation excess of this model of the coil state:

$$\bar{\Gamma}_C = \frac{1}{2} - \sqrt{\frac{1}{4} + \left(\frac{ce}{\rho}\right)^2} - \frac{ce}{\rho}, \tag{10}$$

where c is the salt concentration in the bulk, e is the fundamental charge and ρ is the absolute value of the uniform volume charge density.

It is possible to connect this model to physical NA coils via the charge density parameter. If we treat the NA coil as a sphere, with charge Q and radius R, then $\rho = \frac{Q}{(4/3)\pi R^3}$ or, using the definition of the radius of gyration, R_g,

$$\rho = \frac{Q}{\frac{4}{3}\left(\frac{5}{3}\right)^{\frac{3}{2}} \pi R_g^3}. \tag{11}$$

Salt-dependent R_g values for dT_{50} have been measured using small-angle X-ray scattering by Sim *et al.* (51); we are not aware of similar measurements for RNA. We can insert these R_g values into Equation (11) and, in turn, into Equation (10) to obtain semi-theoretical predictions of $\bar{\Gamma}_C$ based on the uniform mean-field (UMF) model and the experimental R_g values. These predictions are co-plotted with the molal data in Figure 5A.

This simple, UMF model exhibits $\bar{\Gamma}_C \to 0.5$ high-salt limiting behaviour (Supplementary Figure S10); however, its quantitative agreement with the experimental data is poor. Our hypothesis of dominant conformational flexibility, leading the system to behave as if it is uniformly charged, is thus not borne out. We require an alternative model, including some non-uniformity in the charge distribution, to explain the data.

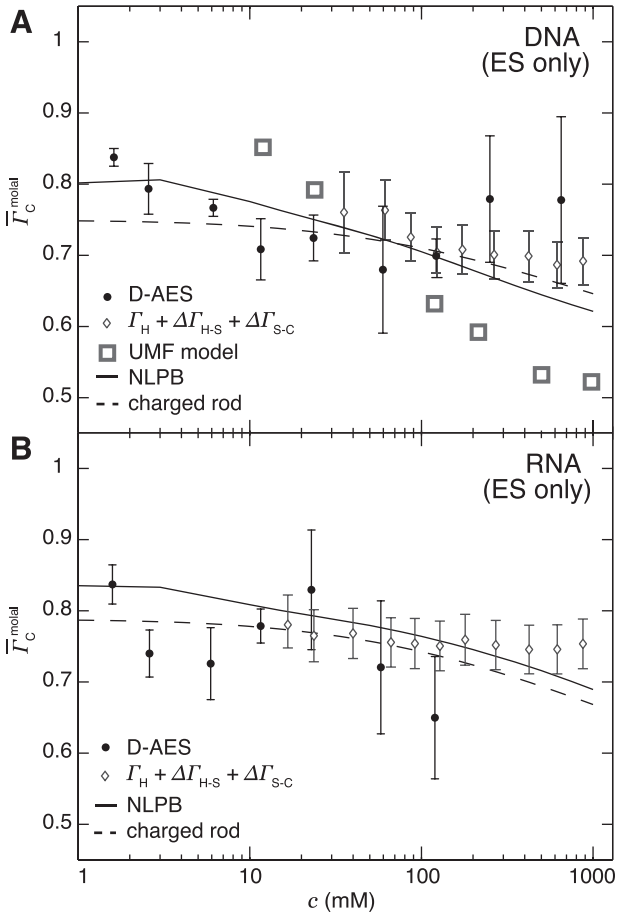

Figure 5. Comparison of uniform mean-field model (open squares), naive NLPB calculations (solid line) and charged rod model (dashed line) to D-AES (points) and single-molecule (open diamonds) data for (**A**) DNA and (**B**) RNA. Shown are values of $\bar{\Gamma}_C^{\text{molal}}$; i.e. corrected for the EV effect to emphasize electrostatics.

Non-uniform mean-field models

Because all of our experiments are carried out in the presence of added salt, ES interactions will be appreciable only on length scales shorter than the Debye screening length, κ^{-1}. The conformational flexibility that is central to the UMF model occurs only on long length scales compared with κ^{-1}. As such, we now hypothesize that it is the short-length-scale (i.e. sub-Debye-length) charge distribution of the system, which is rod-like, that dominates the interactions with the ion atmosphere.

One way to account for the local charge distribution in the ssNA coil is through the single-stranded NLPB calculations of Figure 4C, which are based on a naive structural model (Figure 4B) that does not sample the available conformations of the chain but does account for the discreteness of the source charge and its spacing along the backbone. Because this naive model is based on the canonical double-helical structure, it incorporates some degree of base-stacking, not present in the random-coil dT_{50} or rU_{50}, that may introduce error into the modelling. Figure 5 compares these NLPB results with the molal DNA and RNA data, showing good agreement across the full range of salt concentration in both cases.

An alternative, structurally simpler model lacking discrete charges is that of Landy *et al.* (52), in which the NA is treated as a charged rod with radius a. In the low ionic strength, excess salt limit, this model predicts that the cation excess of the negatively charged rod is given by

$$\bar{\Gamma} \approx \frac{\xi - 1/2}{2\xi}\left[1 - \left(\frac{K_0(\kappa a)}{K_1(\kappa a)}\right)^2\right] + \frac{1}{2}, \qquad (12)$$

where ξ is the Manning parameter (17) ($\xi = 1$ for ssDNA, $\xi = 1.19$ for ssRNA), κ^{-1} is the Debye length and the K_i are the modified Bessel functions of the second kind; this equation is valid for $\xi \geq 1$. For the ssNAs, the choice of a is non-obvious. Here, for both RNA and DNA, we set $a =$ 0.24 nm: the distance of closest approach of Na^+ ions to the backbone phosphates in molecular dynamics simulations of dsRNA (53). As shown in Figure 5, the charged rod model also agrees with the data except at the very lowest salt concentrations.

That both the single-stranded NLPB and charged rod models agree with the EV-corrected $\bar{\Gamma}_C^{\text{molal}}$ data indicates that the monovalent ion excess of ssNAs is insensitive to their large-length-scale conformation. Rather, it is the spacing of the charges along the strand that dominates. This effect is seen by comparing the $\bar{\Gamma}_C$ results for RNA (0.59 nm spacing along sugar-phosphate backbone) and DNA (0.70 nm spacing) in Figures 3 and 5. That the ion excess is insensitive to the conformation of the NA is consistent with the small magnitude of $\Delta\bar{\Gamma}_{S-C}$, the change in ion excess between two states that differ, primarily, in their conformation (i.e. extended versus coiled). It is also consistent with our hypothesis that, due to ES screening on length scales larger than the Debye length, the interactions between the ion atmosphere and the NA are dominated by the rod-like charge distribution on short length scales.

CONCLUSION

We have presented new D-AES measurements of the absolute number of ions associated with unfolded DNA and RNA oligonucleotides, single-molecule measurements of the change in number of ions associated with an RNA hairpin as it is mechanically unfolded and NLPB calculations of the absolute number of ions associated with double-helical and single-stranded DNA and RNA. Using these results, along with existing data on a number of NA systems, we have obtained three different measurements of the monovalent ion atmosphere, Γ_C, of unfolded, single-stranded DNA and two different measurements of unfolded RNA. We have also reported measurements of the change in ion excess as an unfolded NA folds to form secondary structure. These $\Delta\Gamma_{\text{H-C}}$ results, which show non-trivial salt dependence (Supplementary Figure S7), contribute to understanding the free energy change associated with secondary structure formation.

We interpret the observed salt-dependent Γ_C behaviour as an interpolation between two limiting regimes: a low-salt limit described by Manning counterion condensation theory and a high-salt, Debye–Hückel limit in which the charge is equally offset by cation association and anion depletion. The detailed behaviour at intermediate salt concentrations depends on the strandedness and charge spacing of the NA, but does not depend appreciably on its large-scale conformation, presumedly due to the short-range nature of the screened electrostatics. This indicates that, when considering free energies of ion interactions in the context of NA structure formation, much of the molecular complexity on large length scales can likely be ignored.

SUPPLEMENTARY DATA

Supplementary Data are available at NAR online.

ACKNOWLEDGEMENTS

We thank Alexander Grosberg for proposing the uniform mean-field model, Dan Nguyen and Amanda Strom for experimental assistance and David Draper, Luc Jaeger and Philip Pincus for helpful discussions. AES studies were performed in the NSF-supported MRL TEMPO lab.

FUNDING

National Science Foundation [DMR-1006737, DMR-1309414, DGE-1144085 to D.R.J., DMR-1121053 to the MRL TEMPO lab]. Funding for open access charge: NSF research funding.

Conflict of interest statement. None declared.

REFERENCES

1. Doherty,E.A. and Doudna,J.A. (2000) Ribozyme structures and mechanisms. *Annu. Rev. Biochem.*, **69**, 597–615.
2. Garst,A.D., Edwards,A.L. and Batey,R.T. (2011) Riboswitches: structures and mechanisms. *Cold Spring Harbor Perspect. Biol.*, **3**, a003533.
3. Rothemund,P.W. (2006) Folding DNA to create nanoscale shapes and patterns. *Nature*, **440**, 297–302.

4. Leipply,D., Lambert,D. and Draper,D.E. (2009) Ion–RNA interactions: thermodynamic analysis of the effects of mono- and divalent ions on RNA conformational equilibria. *Method. Enzymol.*, **469**, 433–463.
5. Shack,J., Jenkins,R.J. and Thompsett,J.M. (1952) The binding of sodium chloride and calf thymus desoxypentose nucleic acid. *J. Biol. Chem.*, **198**, 85–92.
6. Strauss,U.P., Helfgott,C. and Pink,H. (1967) Interactions of polyelectrolytes with simple electrolytes. II. Donnan equilibria obtained with DNA in solutions of 1-1 electrolytes. *J. Phys. Chem.*, **71**, 2550–2556.
7. Bai,Y., Greenfeld,M., Travers,K.J., Chu,V.B., Lipfert,J., Doniach,S. and Herschlag,D. (2007) Quantitative and comprehensive decomposition of the ion atmosphere around nucleic acids. *J. Am. Chem. Soc.*, **129**, 14981–14988.
8. Pabit,S.A., Meisburger,S.P., Li,L., Blose,J.M., Jones,C.D. and Pollack,L. (2010) Counting ions around DNA with anomalous small-angle X-ray scattering. *J. Am. Chem. Soc.*, **132**, 16334–16336.
9. Giambaşu,G.M., Gebala,M.K., Panteva,M.T., Luchko,T., Case,D.A. and York,D.M. (2015) Competitive interaction of monovalent cations with DNA from 3D-RISM. *Nucleic Acids Res.*, **43**, 8405–8415.
10. Gebala,M., Giambaşu,G.M., Lipfert,J., Bisaria,N., Bonilla,S., Li,G., York,D.M. and Herschlag,D. (2015) Cation–anion interactions within the nucleic acid ion atmosphere revealed by ion counting. *J. Am. Chem. Soc.*, **137**, 14705–14715.
11. Rix-Montel,M.-A., Grassi,H. and Vasilescu,D. (1974) Experimental studies of thermal denaturation of the Na-DNA system with respect to Manning's model. *Biophys. Chem.*, **2**, 278–289.
12. Okubo,T. and Ise,N. (1969) Mean and single-ion activity coefficients and transference data of the sodium salt of a deoxyribonucleic acid in aqueous solution. *Macromolecules*, **2**, 407–411.
13. Ascoli,F., Botre,C. and Liquori,A. (1961) Irreversible changes of ionic activities following thermal denaturation of sodium deoxyribonucleate. *J. Mol. Biol.*, **3**, 202–207.
14. Meisburger,S.P., Sutton,J.L., Chen,H., Pabit,S.A., Kirmizialtin,S., Elber,R. and Pollack,L. (2013) Polyelectrolyte properties of single stranded DNA measured using SAXS and single-molecule FRET: beyond the wormlike chain model. *Biopolymers*, **99**, 1032–1045.
15. Record,M.T. Jr, Zhang,W. and Anderson,C.F. (1998) Analysis of effects of salts and uncharged solutes on protein and nucleic acid equilibria and processes: a practical guide to recognizing and interpreting polyelectrolyte effects, Hofmeister effects, and osmotic effects of salts. *Adv. Protein Chem.*, **51**, 281–353.
16. Ni,H., Anderson,C.F. and Record,M.T. (1999) Quantifying the thermodynamic consequences of cation (M2+, M+) accumulation and anion (X-) exclusion in mixed salt solutions of polyanionic DNA using Monte Carlo and Poisson-Boltzmann calculations of ion-polyion preferential interaction coefficients. *J. Phys. Chem. B*, **103**, 3489–3504.
17. Manning,G.S. (1969) Limiting laws and counterion condensation in polyelectrolyte solutions I. Colligative properties. *J. Chem. Phys.*, **51**, 924–933.
18. Anderson,C.F. and Record,M.T. (1980) The relationship between the Poisson-Boltzmann model and the condensation hypothesis: an analysis based on the low salt form of the Donnan coefficient. *Biophys. Chem.*, **11**, 353–360.
19. Salamone,J., (ed.) (1996) *Polymeric Materials Encyclopedia*, CRC Press, pp. 649–650.
20. Debye,P. and Hückel,E. (1923) Zur theorie der elektrolyte I: Gefrierpunktserniedrigung und verwandte erscheinungent. *Phys. Z.*, **24**, 185–206.
21. Alexandrowicz,Z. and Katchalsky,A. (1963) Colligative properties of polyelectrolyte solutions in excess of salt. *J. Polym. Sci. Part A*, **1**, 3231–3260.
22. Anderson,C.F. and Record,M.T. Jr (1982) Polyelectrolyte theories and their applications to DNA. *Annu. Rev. Phys. Chem.*, **33**, 191–222.
23. Olmsted,M.C., Anderson,C.F. and Record,M.T. (1991) Importance of oligoelectrolyte end effects for the thermodynamics of conformational transitions of nucleic acid oligomers: a grand canonical Monte Carlo analysis. *Biopolymers*, **31**, 1593–1604.
24. Goddard,N.L., Bonnet,G., Krichevsky,O. and Libchaber,A. (2000) Sequence dependent rigidity of single stranded DNA. *Phys. Rev. Lett.*, **85**, 2400–2403.
25. Seol,Y., Skinner,G.M., Visscher,K., Buhot,A. and Halperin,A. (2007) Stretching of homopolymeric RNA reveals single-stranded helices and base-stacking. *Phys. Rev. Lett.*, **98**, 158103.
26. Chen,H., Meisburger,S.P., Pabit,S.A., Sutton,J.L., Webb,W.W. and Pollack,L. (2012) Ionic strength-dependent persistence lengths of single-stranded RNA and DNA. *Proc. Natl. Acad. Sci. U.S.A.*, **109**, 799–804.
27. Baker,N.A., Sept,D., Joseph,S., Holst,M.J. and McCammon,J.A. (2001) Electrostatics of nanosystems: application to microtubules and the ribosome. *Proc. Natl. Acad. Sci. U.S.A.*, **98**, 10037–10041.
28. Macke,T. and Case,D.A. (1998) Modeling unusual nucleic acid structures. In: Leontes,N.B. and SantaLucia,J. (eds.), *Molecular Modeling of Nucleic Acids*, American Chemical Society, pp. 379–393.
29. Dolinsky,T.J., Czodrowski,P., Li,H., Nielsen,J.E., Jensen,J.H., Klebe,G. and Baker,N.A. (2007) PDB2PQR: expanding and upgrading automated preparation of biomolecular structures for molecular simulations. *Nucleic Acids Res.*, **35**(Suppl 2), W522–W525.
30. Dolinsky,T.J., Nielsen,J.E., McCammon,J.A. and Baker,N.A. (2004) PDB2PQR: an automated pipeline for the setup of Poisson–Boltzmann electrostatics calculations. *Nucleic Acids Res.*, **32**(Suppl 2), W665–W667.
31. Shkel,I.A. and Record,M.T. (2012) Coulombic free energy and salt ion association per phosphate of all-atom models of DNA oligomer: dependence on oligomer size. *Soft Matter*, **8**, 9345–9355.
32. Ribeck,N. and Saleh,O.A. (2008) Multiplexed single-molecule measurements with magnetic tweezers. *Rev. Sci. Instrum.*, **79**, 094301.
33. Dittmore,A., Landy,J., Molzon,A.A. and Saleh,O.A. (2014) Single-molecule methods for ligand counting: linking ion uptake to DNA hairpin folding. *J. Am. Chem. Soc.*, **136**, 5974–5980.
34. Jacobson,D.R. and Saleh,O.A. (2015) Measuring the differential stoichiometry and energetics of ligand binding to macromolecules by single-molecule force spectroscopy: an extended theory. *J. Phys. Chem. B*, **119**, 1930–1938.
35. Landy,J., McIntosh,D. and Saleh,O. (2012) Quantifying screening ion excesses in single-molecule force-extension experiments. *Phys. Rev. Lett.*, **109**, 048301.
36. Todd,B.A. and Rau,D.C. (2008) Interplay of ion binding and attraction in DNA condensed by multivalent cations. *Nucleic Acids Res.*, **36**, 501–510.
37. Zhang,H. and Marko,J.F. (2008) Maxwell relations for single-DNA experiments: monitoring protein binding and double-helix torque with force-extension measurements. *Phys. Rev. E*, **77**, 031916.
38. Donnan,F.G. (1911) Theorie der membrangleichgewichte und membranpotentiale bei vorhandensein von nicht dialysierenden elektrolyten. Ein beitrag zur physikalisch-chemischen physiologie. *Z. Elektrochem. Angew. P.*, **17**, 572–581.
39. Shkel,I.A. and Record,M.T. (2004) Effect of the number of nucleic acid oligomer charges on the salt dependence of stability ($\Delta G_{37}{}^{o}$) and melting temperature (T_m): NLPB analysis of experimental data. *Biochemistry*, **43**, 7090–7101.
40. MacKerell,A.D. (1997) Influence of magnesium ions on duplex DNA structural, dynamic, and solvation properties. *J. Phys. Chem. B*, **101**, 646–650.
41. Tan,Z.-J. and Chen,S.-J. (2006) Nucleic acid helix stability: effects of salt concentration, cation valence and size, and chain length. *Biophys. J.*, **90**, 1175–1190.
42. Jacobson,D.R., McIntosh,D.B. and Saleh,O.A. (2013) The snakelike chain character of unstructured RNA. *Biophys. J.*, **105**, 2569–2576.
43. Reiling,C., Khutsishvili,I., Huang,K. and Marky,L.A. (2015) Loop contributions to the folding thermodynamics of DNA straight hairpin loops and pseudoknots. *J. Phys. Chem. B*, **119**, 1939–1946.
44. Stellwagen,E., Muse,J.M. and Stellwagen,N.C. (2011) Monovalent cation size and DNA conformational stability. *Biochemistry*, **50**, 3084–3094.
45. Williams,D.J. and Hall,K.B. (1996) Thermodynamic comparison of the salt dependence of natural RNA hairpins and RNA hairpins with non-nucleotide spacers. *Biochemistry*, **35**, 14665–14670.
46. Bond,J.P., Anderson,C.F. and Record,M.T. Jr (1994) Conformational transitions of duplex and triplex nucleic acid helices: thermodynamic analysis of effects of salt concentration on stability using preferential interaction coefficients. *Biophys. J.*, **67**, 825–836.
47. Record,M.T. (1975) Effects of Na+ and Mg++ ions on the helix–coil transition of DNA. *Biopolymers*, **14**, 2137–2158.

48. Record,M.T. (1967) Electrostatic effects on polynucleotide transitions. II. Behavior of titrated systems. *Biopolymers*, **5**, 993–1008.
49. Owczarzy,R., You,Y., Moreira,B.G., Manthey,J.A., Huang,L., Behlke,M.A. and Walder,J.A. (2004) Effects of sodium ions on DNA duplex oligomers: improved predictions of melting temperatures. *Biochemistry*, **43**, 3537–3554.
50. Record,M.T., Anderson,C.F. and Lohman,T.M. (1978) Thermodynamic analysis of ion effects on the binding and conformational equilibria of proteins and nucleic acids: the roles of ion association or release, screening, and ion effects on water activity. *Q. Rev. Biophys.*, **11**, 103–178.
51. Sim,A.Y., Lipfert,J., Herschlag,D. and Doniach,S. (2012) Salt dependence of the radius of gyration and flexibility of single-stranded DNA in solution probed by small-angle x-ray scattering. *Phys. Rev. E*, **86**, 021901.
52. Landy,J., Lee,Y. and Jho,Y. (2013) Limiting law excess sum rule for polyelectrolytes. *Phys. Rev. E*, **88**, 052315.
53. Kirmizialtin,S., Silalahi,A.R., Elber,R. and Fenley,M.O. (2012) The ionic atmosphere around A-RNA: Poisson-Boltzmann and molecular dynamics simulations. *Biophys. J.*, **102**, 829–838.